Biphoton wave packets in parametric down-conversion: Spectral and temporal structure and degree of entanglement

Yu. M. Mikhailova,[1,2] P. A. Volkov,[1] and M. V. Fedorov[1,*]
[1]*A.M. Prokhorov General Physics Institute, Russian Academy of Sciences, 38 Vavilov Street, Moscow, 119991, Russia*
[2]*Max-Planck-Institut für Quantenoptik, Hans-Kopfermann-Strasse 1, D-85748, Garching, Germany*
(Received 19 August 2008; published 16 December 2008)

We investigate spectral and temporal features and entanglement of biphoton wave packets formed in spontaneous parametric down-conversion with a pulsed laser pump. The degree of entanglement is characterized by the experimentally measurable parameter R defined as the ratio of the coincidence and single-particle spectral widths. In the frequency representation, this parameter is found as a function of the pump-pulse duration τ. The function $R(\tau)$ is shown to have a minimum and even in the minimum, at rather natural conditions, the degree of entanglement is found to be very high ($R_{\min}=73$). The Schmidt number K is found analytically for both short and long pump pulses and interpolated for arbitrary pulse durations. All functional dependences of R and K are found to be identical and numerical coefficients are found to be rather close. Two-time temporal wave function of a biphoton state is investigated in detail, and a rather significant difference between the cases of short and long pump pulses is found to occur. In the case of long pulses, the temporal parameter R_t (defined as the ratio of durations of the single-particle and coincidence signals) is shown to be very close to the Schmidt number K.

DOI: 10.1103/PhysRevA.78.062327 PACS number(s): 03.67.Bg, 03.67.Mn, 42.65.Lm

I. INTRODUCTION

Entanglement is a fundamental feature of multipartite systems characterizing the degree of correlations between particles. Entangled states find their wide application in quantum information, quantum cryptography, and related topics. Spontaneous parametric down-conversion (SPDC) is one of the most often used processes for production of entangled biphoton states. The most popular and widely discussed type of entanglement of SPDC states is the entanglement with respect to polarization variables. On the other hand, in addition to polarization, SPDC photons are characterized also by other degrees of freedom, such as angles determining directions of propagation and lengths of wave vectors (or frequencies) of photons. In contrast to polarization, these degrees of freedom belong to the class of continuous variables. Multi- and bipartite states with continuous variables are quite attractive because they correspond to an infinitely high dimensionality of the Hilbert space and, potentially, their degree of entanglement can be very high; but in practice, of course, there are limitations. Nevertheless, there are conditions when the degree of entanglement with respect to continuous variables can be really high, much higher than the maximal achievable degree of entanglement with respect to discrete variables. For example, in Ref. [1] SPDC biphoton states were shown to be highly entangled with respect to angular variables. Spectral features of highly entangled SPDC biphoton states were also investigated in some works in the cases of short pulses [2] and a cw laser pump [3]. However, the degree of entanglement was neither defined nor discussed. Definition of the most appropriate entanglement quantifiers and evaluation of the degree of entanglement in a wide range of pump-pulse durations is one of the key goals of this work.

We characterize the degree of entanglement by the recently introduced [4] parameter R defined as the ratio of widths of single-particle and coincidence wave packets. We find R analytically in two asymptotic cases of short and long pump pulses (with the parameter separating these two regions explicitly defined) and we show that in these two cases R is extremely high ($\sim$300 or more). By using both interpolation formulas and exact numerical calculations we show that in the case of the type-I phase matching we consider, R is very high ($\sim$70) even in the most unfavorable case of intermediately long pump pulses ($\sim$1 ps).

In contrast to all other entanglement quantifiers, the parameter R is rather easy experimentally measurable. For double-Gaussian bipartite states the parameter R is known [5] to coincide with such a well-known entanglement quantifier as the Schmidt number K. However, the wave functions characterizing the biphoton frequency distributions are rather far from the double-Gaussian ones. Nevertheless, as we show in this paper, even for such functions the parameters R and K are very close to each other. By using specific features of the biphoton wave functions we calculate in Sec. V the Schmidt number explicitly in both cases of short and long pump pulses and we find that in both cases all functional dependences of R and K are identical, and there is only a small difference between them in numerical coefficients. This means that the parameter R is, indeed, an appropriate quantifier of entanglement which can be both found theoretically and measured experimentally.

In addition to spectral analysis we describe also a temporal structure of the SPDC biphoton wave packet determined by its two-time wave function. This structure has many very interesting features. We derive a series of very simple formulas, which are used to explain and characterize analytically parameters of the calculated temporal envelopes of single-particle and coincidence signals. We find that features of these curves are qualitatively different in the cases of short

*fedorov@ran.gpi.ru

and long pump pulses. In the case of short pump pulses duration of coincidence temporal signals is shown to be varying in very large limits with varying time of observation, and this makes the temporal picture with short pump pulses inappropriate for defining the temporal parameter R, R_t. In contrast, in the case of long pump pulses, duration of coincidence temporal signals is shown to be independent of the observation time, the parameter R_t is well-defined and is shown to be very close to the Schmidt number K.

II. GENERAL FORMULAS

SPDC is the process in which a classical pump wave propagates through a birefringent crystal, where some photons of the pump are absorbed and give rise to the birth of two photons of smaller frequencies, signal and idler. If $\mathbf{k_1}$ and $\mathbf{k_2}$ are wave vectors of emitted photons, the QED state arising in the SPDC process is given by the sum of the vacuum state and superposition of two-photon states,

$$|\mathrm{SPDC}\rangle = |\mathrm{vac}\rangle + \sum_{\mathbf{k}_1,\mathbf{k}_2} \Psi(\mathbf{k}_1,\mathbf{k}_2)|\mathbf{k}_1,\mathbf{k}_2\rangle, \tag{1}$$

where $|\mathbf{k_1},\mathbf{k_2}\rangle = \mathbf{a}^\dagger_{\mathbf{k_1}}\mathbf{a}^\dagger_{\mathbf{k_2}}|\mathrm{vacuum}\rangle$, $a^\dagger_{\mathbf{k}}$ is the operator of creation of a photon in a state with the momentum (wave vector) $\mathbf{k}$, and $\Psi(\mathbf{k_1},\mathbf{k_2})$ is the biphoton wave function in the momentum representation. General expressions for this wave function are well-known [6,7], and for pump pulses of a finite duration the biphoton wave function can be written in the form

$$\Psi(\mathbf{k}_{1\perp},\mathbf{k}_{2\perp};\omega_1,\omega_2) = \chi \int d\mathbf{r} \int dt \int d\mathbf{k}_{p\perp} \int d\omega_p E_p(\mathbf{k}_{p\perp},\omega_p)\exp[i(\mathbf{k}_{p\perp}-\mathbf{k}_{1\perp}-\mathbf{k}_{2\perp})\cdot\mathbf{r}_\perp + i\boldsymbol{\Delta}\cdot z]\exp[i(\omega_1+\omega_2-\omega_p)t], \tag{2}$$

where χ is the crystal susceptibility, indices p and $\perp$ indicate, correspondingly, the pump and the plane perpendicular to the laser axis (z axis), E_p is the Fourier transform of the electric field amplitude of the pump, and Δ is the longitudinal mismatch,

$$\Delta = \sqrt{\frac{n_p^2\omega_p^2}{c^2} - \mathbf{k}_{p\perp}^2} - \sqrt{\frac{n_1^2\omega_1^2}{c^2} - \mathbf{k}_{1\perp}^2} - \sqrt{\frac{n_2^2\omega_2^2}{c^2} - \mathbf{k}_{2\perp}^2}, \tag{3}$$

n_p, n_1, and n_2 are the refractive indices of the pump and emitted photons.

Let us make now a series of simplifying assumptions and approximations. Let us consider the type-I SPDC decay process $e \to o+o$, in which both emitted photons belong to the ordinary wave and, hence, $n_1=n_2=n_o$. Integration over time t in Eq. (2) from $-\infty$ to ∞ gives $2\pi\delta(\omega_p-\omega_1-\omega_2)$, with which the integral over ω_p can be easily taken. Similarly, in the wide-crystal approximation the limits of integration over $\mathbf{r}_\perp$ can be extended to $-\infty$ and ∞ in both transverse directions which gives $(2\pi)^2\delta(\mathbf{k}_{p\perp}-\mathbf{k}_{1\perp}-\mathbf{k}_{2\perp})$, and this can be used to take the integral over $\mathbf{k}_{p\perp}$. Let us restrict our consideration in this work only by the case of a purely collinear propagation of emitted photons, in which $\mathbf{k}_{1\perp}=\mathbf{k}_{2\perp}=0$ and, hence, $\mathbf{k}_{p\perp}=0$. Besides, let us consider here only the case of degenerate central frequencies $\omega_1^{(0)}$ and $\omega_2^{(0)}$, $\omega_1^{(0)}=\omega_2^{(0)}=\omega_0/2$, where ω_0 is the central frequency of the pump. We will assume also that deviations from these central frequencies, $\nu_{1,2}\equiv\omega_{1,2}-\omega_{1,2}^{(0)}$, are small: $|\nu_{1,2}| \ll \omega_0$. Finally, we will take the spectral amplitude of the pump in a Gaussian form

$$\begin{aligned} E_p(\mathbf{k}_{p\perp}=0,\omega_p) &\equiv E_p(\omega_p) \\ &= E_0 \exp\left[-\frac{(\omega_p-\omega_0)^2\tau^2}{8\ln 2}\right] \\ &= E_0 \exp\left[-\frac{(\omega_1+\omega_2-\omega_0)^2\tau^2}{8\ln 2}\right], \end{aligned} \tag{4}$$

where τ is the duration of pump pulses and $\omega_p=\omega_1+\omega_2=\omega_0+\nu_1+\nu_2$.

Under the formulated assumptions and approximations Eq. (2) for the biphoton wave function is reduced to a much simpler form,

$$\Psi(\omega_1,\omega_2) \propto E_p(\omega_1+\omega_2)\int_0^L dz e^{i\Delta(\omega_1,\omega_2)z} \tag{5}$$

or, after integration over z,

$$\Psi(\omega_1,\omega_2) \propto E_p(\omega_1+\omega_2)\mathrm{sinc}\left[\frac{L}{2}\Delta(\omega_1,\omega_2)\right], \tag{6}$$

where $\mathrm{sinc}(u)=\sin u/u$, L is the length of the crystal (along the laser axis), and the phase mismatch $\Delta(\omega_1,\omega_2)$ is determined by the equation following from Eq. (3),

$$\begin{aligned} \Delta &= k_p - k_1 - k_2 \\ &= \frac{(\omega_1+\omega_2)n_p(\omega_1+\omega_2) - \omega_1 n_0(\omega_1) - \omega_2 n_0(\omega_2)}{c}. \end{aligned} \tag{7}$$

Note that as we will be interested mainly in shapes and widths of photon spectral distributions, in Eqs. (5) and (6) and henceforth we drop all the constant coefficients on the right-hand sides of such equations by using the proportionality symbol. If not specified differently, all curves describ-

ing spectral or temporal distributions will be normalized by the condition of being equal to unity at maxima.

Owing to the assumption about small deviations of frequencies $\omega_{1,2}$ from $\omega_{1,2}^{(0)}$, the expression on the right-hand side of Eq. (7) can be expanded in powers of ν_1 and ν_2 with only two lowest orders to be taken into account,

$$\Delta \approx \frac{1}{c}\left[A(\nu_1+\nu_2) - 2B\frac{\nu_1^2+\nu_2^2}{\omega_0}\right], \tag{8}$$

where A is the dimensionless constant characterizing the temporal walk-off

$$A = c[\,k_p'(\omega)|_{\omega=\omega_0} - \,k_1'(\omega)|_{\omega=\omega_0/2}] = c\left(\frac{1}{v_g^{(p)}} - \frac{1}{v_g^{(o)}}\right); \tag{9}$$

$v_g^{(p)}$ and $v_g^{(o)}$ are the group velocities of the pump and ordinary waves, calculated at wavelengths λ_0 and $2\lambda_0$, correspondingly; $v_g^{(o)} > v_g^{(p)}$. B in Eq. (8) is the dispersion constant, also dimensionless,

$$B = \frac{c}{4}\omega_0\, k_1''(\omega)|_{\omega=\omega_0/2}. \tag{10}$$

For a $LiIO_3$ crystal and $\lambda_0=400$ nm numerical values of the constants A and B are $A=0.17$ and $B=0.069$. Though small, nevertheless, the quadratic term in Eq. (8) is crucially important for determining finite width of the photon single-particle distribution (see Sec. III B). Note also that in Eq. (8) we have dropped the dispersion arising from the wave vector of the pump which is proportional to $k_p''(\nu_1+\nu_2)^2$. This term is dropped because it depends on the same combination of frequencies as the linear term $\nu_1+\nu_2$ and determines only a small correction to the linear term not changing qualitatively its functional dependence on ν_1 and ν_2. In the same approximation we can further simplify the dispersion term taken into account in Eq. (8): $\nu_1^2+\nu_2^2 \equiv \frac{1}{2}[(\nu_1+\nu_2)^2+(\nu_1-\nu_2)^2] \to \frac{1}{2}(\nu_1-\nu_2)^2$. With this substitution the final expression for the biphoton wave function takes the form

$$\Psi(\nu_1,\nu_2) \propto \exp\left(-\frac{(\nu_1+\nu_2)^2\tau^2}{8\ln 2}\right) \times \mathrm{sinc}\left\{\frac{L}{2c}\left[A(\nu_1+\nu_2) - B\frac{(\nu_1-\nu_2)^2}{\omega_0}\right]\right\}. \tag{11}$$

III. COINCIDENCE AND SINGLE-PARTICLE DISTRIBUTIONS (SHORT PULSES)

A. Coincidence spectrum

The coincidence spectrum is determined by the squared wave function $|\Psi(\nu_1,\nu_2)|^2$ of Eq. (11) at a given value of ν_2. For practical purposes, it is more convenient to consider the coincidence and single-particle probability densities as functions of wavelengths $\lambda_{1,2}$ rather than frequencies $\nu_{1,2}=2\pi c/\lambda_{1,2}-\pi c/\lambda_0$. For the crystal length and pump-pulse duration equal to $L=0.5$ cm and $\tau=50$ fs, the coincidence spectral distribution $dw^{(c)}/d\lambda_1$ is characterized by the narrow

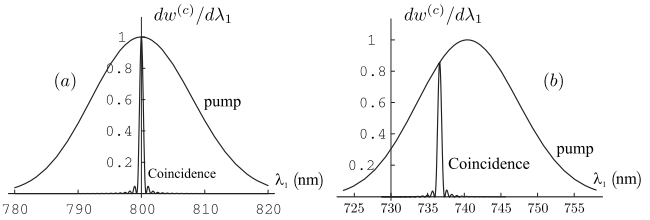

FIG. 1. Normalized coincidence and pump spectra (narrow and wide curves) as functions of λ_1 at λ_2=(a) 800 nm and (b) 870 nm.

curves of Fig. 1. The wide curves in the pictures of Fig. 1 describe the pump spectrum. The curves of the pictures (a) and (b) are calculated at the second-photon wavelength λ_2 taken equal to 800 and 870 nm.

Figure 1 clearly shows that (i) the coincidence spectrum is much narrower than that of the pump and (ii) the coincidence spectral width $\Delta\lambda_1^{(c)}$ does not depend on λ_2. If we take the wavelength of the second photon exactly equal to the double pump wavelength, $\lambda_2=2\lambda_0=800$ nm, the peaks of the pump and coincidence spectra coincide and are located at $\lambda_1=800$ nm [Fig. 1(a)]. If we shift λ_2 to the right, both pump and coincidence spectra move to the left from the point $\lambda_2=800$ nm. However, for the coincidence spectral distribution this shift is slightly larger than for the pump. For this reason the amplitude of the coincidence signal appears to be somewhat smaller than in the case of location at 800 nm. However, the width of the coincidence spectral distribution remains practically the same as in the case $\lambda_2=800$ nm. Hence the coincidence spectral width $\Delta\lambda_1^{(c)}$ is a constant parameter, independent of tuning of the second-photon detector.

Analytically the coincidence spectral width can be easily found directly from Eq. (11). In the case of short pulses the Gaussian function in this equation is much narrower than the sinc function. For bipartite wave functions having the form of a product of two functions, one of which is much narrower than another, the coincidence distribution is determined by the narrower factor, i.e., in our case by the sinc function. Evidently, its width with respect to varying ν_1 at a given value of ν_2 is given by

$$\Delta\nu_1^{(c)} = \Delta\nu_{1\mathrm{sinc}} = \frac{2.78\times 2c}{AL}, \tag{12}$$

where the factor 2.78 is the full width at half-maximum (FWHM) of the function $\mathrm{sinc}^2(u)$. Numerically, at $L=0.5$ cm, in terms of wavelengths, both analytical expression and results of calculations shown in Fig. 1 correspond to $\Delta\lambda_1^{(c)}=0.658$ nm. For comparison, FWHM of the pump spectral function $\exp[-(\nu_1+\nu_2)^2\tau^2/4\ln 2]$ at a given ν_2 equals

$$\Delta\nu_{1\mathrm{pump}} = \frac{4\ln 2}{\tau}, \tag{13}$$

which gives (in terms of wavelengths, at $\tau=50$ fs and $\lambda_0=400$ nm) $\Delta\lambda_1^{(p)}=2\lambda_0^2\Delta\nu_{1\ \mathrm{pump}}/\pi c=18.8$ nm. In other words, the pump spectrum considered as a function of λ_1,

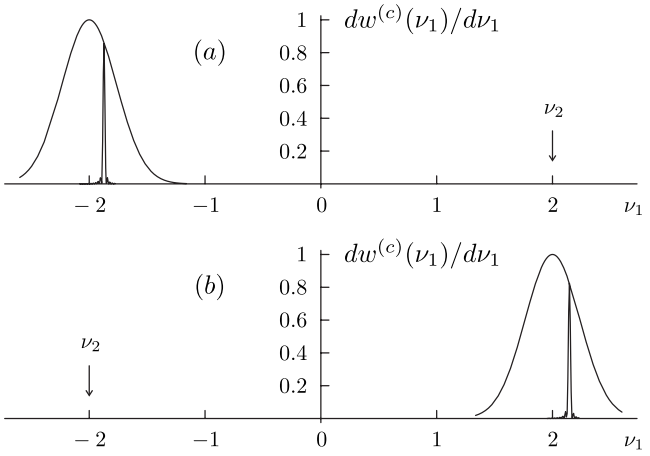

FIG. 2. Normalized coincidence and pump spectra $dw^{(c)}(\nu_1)/d\nu_1$ at (a) $\nu_2=2$ and (b) $\nu_2=-2$, ν_1 and ν_2 are in units of 10 fs.

$$E_p^2 \propto \exp\left\{-\frac{\pi^2 c^2 \tau^2}{\ln 2}\left(\frac{1}{\lambda_1}+\frac{1}{\lambda_2}-\frac{1}{\lambda_0}\right)^2\right\},$$

is 28.57 times wider than the coincidence spectrum.

As shown below, the ratio of the "sinc" and "pump" widths [Eqs. (12) and (13)] determines the parameter separating the regions of short and long pulses,

$$\eta = \frac{\Delta\nu_{1\text{sinc}}}{\Delta\nu_{1\text{pump}}} \approx 2\frac{c\tau}{AL} = \frac{2\tau}{L/vg^{(p)} - L/v_g^{(o)}}. \tag{14}$$

The last expression on the right-hand side of this equation shows that η equals the ratio of the double pump-pulse duration to the difference of times during which a crystal is crossed by the pump and idler-signal photons. Also η can be considered as the dimensionless pump-pulse duration. In SPDC the pump pulses are short if $\eta \ll 1$ and long if $\eta \gg 1$. The boundary pulse duration occurs at $\eta \sim 1$. At $L=0.5$ cm the equality $\eta=1$ yields $\tau=1.43$ ps. As shown below, η is also the key control parameter, determining a value of the entanglement parameter R.

Noncoincidence of the peaks of the pump and coincidence spectra seen in Fig. 1(b) deserves a special comment. For clarification of its origin, it is worth returning to the frequency pictures. In Fig. 2 the coincidence and pump spectra are shown as functions of ν_1 under the conditions when the detector registering the second photon of the pair ("2") is tuned to frequencies shifted as compared to ω_0 (or ν_2 shifted from zero) (a) to the blue and (b) to the red sides. Both the pump and coincidence spectra also appear to be shifted from ω_0 ($\nu_1=0$), but in the directions opposite to the shift of ω_2. As is seen, the peaks of the pump and coincidence spectra do not coincide at sufficiently large values of these shifts. Interesting enough, in both cases the coincidence peak appears to be located at the right wing of the pump, which corresponds to the left wing in the wavelength picture of Fig. 1. This lack of symmetry between (a) and (b) of Fig. 2 is related to the dispersion and, as we will see in the following section, it is related to asymmetry of the single-particle spectrum. Mathematically the results discussed here follow directly from the definition of the phase-mismatch Δ, e.g., taken in the form (8). Location of the coincidence spectral peaks is determined by the condition $\Delta=0$. This gives a quadratic equation of ν_1, the solution of which is given by

$$\nu_1(\nu_2) = \frac{A\omega_0}{4B} - \sqrt{\left(\frac{A\omega_0}{4B}\right)^2 + \frac{A\omega_0}{2B}\nu_2 - \nu_2^2} \approx -\nu_2 + \frac{4B\nu_2^2}{A\omega_0}. \tag{15}$$

The first and second terms on the right-hand side of this equation have different parity. They are, correspondingly, odd and even functions of ν_2, and this explains the lack of symmetry between (a) and (b) of Fig. 2.

The approximation used in the expansion of the square root in Eq. (15) consists in the assumption $|\nu_2| \ll A\omega_0/8B$, which is satisfied for parameters we use in this paper. Actually, if here the approximate expression for $\nu_1(\nu_2)$ was needed only for getting a simple analytical formula explaining the exact calculations of the spectra in Figs. 1 and 2, later this will be shown to be crucially important, in particular, for calculations of the Schmidt number (Sec. V).

B. Single-particle spectrum and the entanglement parameter for short pump pulses

The single-particle photon spectrum is determined by the squared wave function of Eq. (11) integrated over ν_2,

$$\frac{dw^{(s)}}{d\nu_1} = \int d\nu_2 |\Psi(\nu_1,\nu_2)|^2. \tag{16}$$

As the exact analytical calculation of the integral over ν_2 is hardly possible, let us perform this integration approximately with the narrow sinc^2 function substituted by the δ function $\delta[\nu-\nu(\nu_1)]$, where $\nu=\nu_1+\nu_2$ and $\nu(\nu_1)$ is given by an equation similar to Eq. (15),

$$\nu(\nu_1) = \frac{A\omega_0 + 4B\nu_1 - \sqrt{A^2\omega_0^2 + 8AB\omega_0\nu_1}}{2B} \approx \frac{4B\nu_1^2}{A\omega_0}. \tag{17}$$

By using now ν as the integration variable in Eq. (16) (instead of ν_2), we find immediately the following expression for the single-particle spectrum of emitted photons:

$$\frac{dw^{(s)}(\nu_1)}{d\nu_1} \propto \frac{\exp\left\{-\dfrac{[\nu(\nu_1)]^2\tau^2}{4\ln 2}\right\}}{\sqrt{A^2\omega_0^2 + 8AB\omega_0\nu_1}}. \tag{18}$$

In Fig. 3 the spectral distribution determined by Eq. (18) is shown together with the pump spectrum (correspondingly, the wide and narrow curves).

The FWHM of the wide curve in Fig. 3 equals

$$\Delta\nu_1^{(s)} = \Delta\omega_1^{(s)} = \sqrt{\frac{2A\ln(2)\omega_0}{B\tau}}. \tag{19}$$

Numerically, at $\tau=50$ fs, Eq. (19) yields $\Delta\lambda_1^{(s)}=195$ nm, which is ten times larger than the pump spectral width.

The parameter R defined as the ratio of the single-particle to coincidence spectral widths is easily found from Eqs. (12) and (19) to be given by

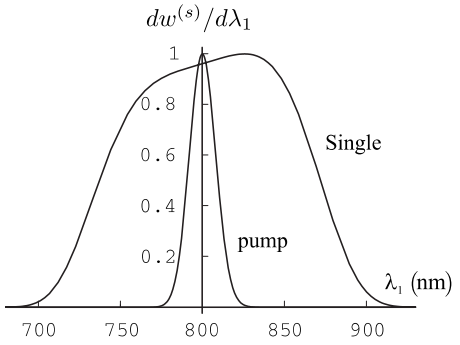

FIG. 3. Single-particle (wide) and pump (narrow) spectra (densities of probability of the corresponding photon distributions).

$$R_{\text{short}} = \frac{\Delta\omega_1^{(s)}}{\Delta\omega_1^{(c)}} = \frac{A^{3/2}}{2.78}\sqrt{\frac{\pi \ln 2}{B}}\frac{L}{\sqrt{\lambda_0 c\tau}} = \frac{\sqrt{2\pi \ln 2}}{2.78}\frac{A}{\sqrt{B\eta}}\sqrt{\frac{L}{\lambda_0}} = 0.7507\frac{A}{\sqrt{B\eta}}\sqrt{\frac{L}{\lambda_0}} = \frac{55.06}{\sqrt{\eta}}, \tag{20}$$

where the subscript "short" emphasizes that this result is valid only for short pump pulses, $\eta \ll 1$, and the control parameter η is defined in Eq. (14). The numerical coefficient 55.06 in the last expression of Eq. (20) was found at the same values of all parameters which were used earlier, except the pump-pulse duration τ which was not fixed yet. At $\tau=50$ fs ($\eta=0.0348$) Eq. (20) yields

$$R_{\text{short}} \approx 295. \tag{21}$$

This degree of entanglement is really high. As it is seen from the given derivation, such an extremely high degree of entanglement is related to two accompanying effects: narrowing of the coincidence and broadening of the single-particle spectra of SPDC photons (compared to the pump spectrum). The second of these two effects is a specific feature of the type-I SPDC process. Indeed, in the case of the type-II pase matching ($o \rightarrow e+o$), in the linear approximation, the expansion of the phase mismatch in powers of ν_1, ν_2 takes the form

$$\Delta = \left(k_p' - \frac{k_1' + k_2'}{2}\right)(\nu_1 + \nu_2) - \frac{k_1' - k_2'}{2}(\nu_1 - \nu_2). \tag{22}$$

As in the case of the type-II phase matching the emitted photons "1" and "2" are different (o and e waves), derivatives of their wave vectors over frequencies are different too, $k_1' \neq k_2'$. For this reason, the phase mismatch of Eq. (22) already in the linear approximation appears to be depending on both the sum and difference of frequencies, $\nu_1+\nu_2$ and $\nu_1-\nu_2$. In this case the linear approximation in ν_1, ν_2 is sufficient for determining finite widths of both coincidence and single-particle distributions. If $k_1'-k_2'$ is of the same order as $k_1'+k_2'$, the difference between the single-particle widths and that of the pump spectrum is not too large. that is, the effect of broadening of the single-particle distribution is missing or is only weakly pronounced. In contrast to this, in the case of the type-I phase matching both emitted photons belong to the same ordinary type of wave and, hence, $k_1'=k_2'$. In the linear approximation the dependence of the phase mismatch Δ [Eq. (22)] on the difference of frequencies $\nu_1-\nu_2$ disappears, and the linear approximation appears to be insufficient for determining the finite width of the single-particle distribution. To define this width one has to take into account the second order (dispersion) term in the expansion of Δ in powers of ν_1, ν_2. As this term is rather small, the width of the single-particle distribution appears to be rather large. That is, equality of k_1' and k_2' gives rise to the above-described broadening of the single-particle spectrum compared to that of the pump. This effect provides at least the ten-fold increase of the parameter R compared to what can be achieved in the type-II SPDC process.

Note that the above-described difference between the type-I and type-II SPDC processes was understood rather long ago [8,9]. Elements of our consideration consist in demonstration of the importance of this effect for producing biphoton states with extremely high degree of entanglement and in explicit evaluation of the achievable degree of entanglement. Concerning other earlier works, in the SPDC process with the type-I phase matching and short pump pulses (~60 fs) highly entangled biphoton states were observed in Ref. [2] but, however, the degree of entanglement was not evaluated. In the work [10] both coincidence and single-particle SPDC spectra were measured simultaneously in the case of SPDC with the type-II phase matching; but analysis of these data indicates that the single-particle spectrum was only twice wider than the coincidence one (which corresponds to $R \sim 2$). In Ref. [11] the degree of spectral entanglement for the type-II SPDC process was evaluated theoretically with the help of decomposition of the wave function in a series of products of Schmidt modes, which is different from our approach. In this work we discuss only possibilities of direct measurements of the coincidence and single-particle spectral and temporal distributions of photons. We do not discuss here connections between results obtained in such a way with interference measurements, e.g., in Refs. [12–17]. We hope to return to this problem elsewhere.

To conclude this section, it is worth mentioning once again that in this work we restrict our consideration by the collinear degenerate SPDC process. We will consider nondegenerate and noncollinear cases elsewhere. Here we would like to mention only that the case considered in this paper is optimal. Any deviations from the collinearity and degeneracy lessen the achievable degree of entanglement. For practical purposes it is important to know how quick is this lessening or, in other words, how robust are the results we derive here with respect to, e.g., increasing angular aperture of detectors. By increasing aperture one increases efficiency of measurements but, maybe, lessens the degree of entanglement. Evidently, requirements of a good collinearity and sufficiently large amount of photons to be registered are opposite. We hope to return to analysis of this dilemma later. Though experimental observability of our results does not cause any doubts.

IV. LONG PUMP PULSES AND INTERPOLATION FOR ARBITRARY PULSE DURATIONS

Until now we have assumed that the sinc function in Eq. (11) is much narrower than the Gaussian function. This is absolutely true, e.g., for the pulse duration $\tau=50$ fs, which was chosen for estimates and illustrations. However, if the pulse duration is significantly longer, the relation between the two functions on the right-hand side of Eq. (11) may be reversed: the Gaussian function can become much narrower than the sinc function. In this case the coincidence distribution is determined by the pump spectrum. For example, for $\nu_2=0$ it has the form

$$\frac{dw^{(c)}}{d\nu_1} \propto \exp\left[-\frac{\nu_1^2\tau^2}{4\ln 2}\right]. \tag{23}$$

In the integral (16) determining the single-particle probability density, the narrow pump spectrum can be approximated by $\delta(\nu_2+\nu_2)$ to give

$$\frac{dw^{(s)}}{d\nu_1} \propto \left\{\mathrm{sinc}\left[\frac{2LB\nu_1^2}{c\omega_0}\right]\right\}^2. \tag{24}$$

The coincidence and single-particle width found from Eqs. (23) and (24) are equal to

$$\Delta\nu_{1\ \mathrm{long}}^{(c)} = \frac{4\ln 2}{\tau}, \quad \Delta\nu_{1\ \mathrm{long}}^{(s)} = \sqrt{\frac{2.78c\omega_0}{LB}}, \tag{25}$$

and the corresponding entanglement parameter R is given by

$$\begin{aligned} R_{\mathrm{long}} &= \frac{\Delta\nu_{1\mathrm{long}}^{(s)}}{\Delta\nu_{1\mathrm{long}}^{(c)}} = \frac{\sqrt{2.78\pi}}{2^{3/2}\ln 2}\frac{c\tau}{\sqrt{BL\lambda_0}} \\ &= \frac{\sqrt{2.78\pi}}{2^{5/2}\ln 2}\frac{A\eta}{\sqrt{B}}\sqrt{\frac{L}{\lambda_0}} \\ &= 0.7537\frac{A\eta}{\sqrt{B}}\sqrt{\frac{L}{\lambda_0}} = 55.28\eta. \end{aligned} \tag{26}$$

The entanglement parameter R_{long} (26) is a linearly growing function of the pulse duration τ. For example, at $\tau=7$ ps Eq. (26) yields $\eta\approx 4.87$ and $R_{\mathrm{long}}\approx 269\gg 1$.

Note that the linear dependence of R_{long} on τ arises because the coincidence spectral width of Eq. (25) is on the order of the inverse pump-pulse duration, $\Delta\nu_{1\mathrm{long}}^{(c)}\sim 1/\tau$, which is true only for Fourier limited pump pulses and becomes wrong in the case of very long pulses or a cw pump laser. In these cases the pump bandwidth $\Delta\omega$ becomes determined by factors different from the inverse pulse duration, and $\Delta\nu_{1\ \mathrm{long}}^{(c)}$ in the definition of R_{long} (26) has to be replaced by $\Delta\omega$ to give

$$R_{\mathrm{cw}} \sim c/(\Delta\omega\sqrt{L\lambda_0 B}). \tag{27}$$

SPDC biphoton states with high spectral entanglement and cw pump were observed in the work [3] where, however, the degree of entanglement was not evaluated.

For evaluating the entanglement parameter $R(\tau)$ in the whole range of variation of the pump-pulse duration (from short- to long-pulse regions) we use the simplest interpolation formula

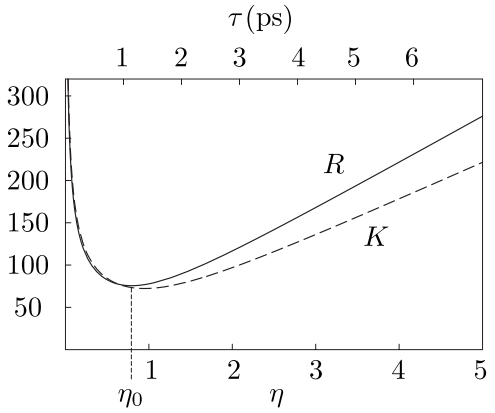

FIG. 4. The parameter R and K vs the control parameter η [Eq. (14)].

$$R(\tau) = \sqrt{R_{\mathrm{short}}^2(\tau) + R_{\mathrm{long}}^2(\tau)}. \tag{28}$$

Note that there is an amusing, though approximate, coincidence relation between numerical coefficients in Eqs. (20) and (26): $\sqrt{2\pi\ln 2}/2.78\approx 1.004\sqrt{2.78\pi}/(2^{5/2}\ln 2)$. Hence with a very good accuracy we can take coefficients in Eqs. (20) and (26) coinciding with each other to get

$$R(\eta) = 0.75\frac{A}{\sqrt{B}}\sqrt{\frac{L}{\lambda_0}}\sqrt{\eta^2+\frac{1}{\eta}} = 55\sqrt{\eta^2+\frac{1}{\eta}}. \tag{29}$$

The function $R(\eta)$ is plotted in Fig. 4.

The curve has a minimum at $\eta_0=2^{-1/3}=0.79$, which corresponds to $\tau_0=1.14$ ps, and in the minimum

$$R_{\mathrm{min}} = R(\tau_0) \approx \frac{A}{\sqrt{B}}\sqrt{\frac{L}{\lambda_0}} \approx 73 \gg 1. \tag{30}$$

So, the parameter $R(\tau)$ is very large and the degree of entanglement is very high in both earlier considered cases of short and long pump pulses, $\tau\ll\tau_0$ and $\tau\gg\tau_0$; but $R(\tau)$ is large and entanglement is high also in the most unfavorable case of intermediate pump-pulse durations around τ_0. Actually, the value of $R(\tau)$ around its minimum is determined by the well-defined parameter equal to the square root of the ratio "length of the crystal divided by the pump wavelength." This result shows that in the type-I degenerate collinear SPDC process, practically, *spectral entanglement is never small*.

V. SCHMIDT NUMBER

As mentioned above (in the Introduction), in the case of double-Gaussian wave functions, the parameter R coincides identically with the Schmidt number K [5], which is widely recognized to be a good quantifier of the degree of entanglement in pure bipartite states. However, the wave function of the form (11) is not double-Gaussian. Actually, if the pump spectral amplitude can be taken Gaussian, the sinc function with the argument containing both linear and quadratic terms in variables $\nu_{1,2}$ cannot be even modeled by any Gaussian form. For this reason, the question that often arises is

whether the parameter R can be used as the entanglement quantifier for states characterized by such non-double-Gaussian wave functions, while the relation between R and K remains unknown. The question is reasonable and, to be answered, it requires the Schmidt number to be explicitly calculated. The solution of this problem is given below.

Let us use the well-known general integral definition of the Schmidt number for bipartite systems with continuous variables [Eq. (10) of Ref. [5]]. In the case of spectral entanglement this definition takes the form

$$K = N^2\left[\int d\nu_1 d\nu_2 d\nu_1' d\nu_2' \Psi(\nu_1,\nu_2)\Psi(\nu_1,\nu_2') \times \Psi(\nu_1',\nu_2)\Psi(\nu_1',\nu_2')\right]^{-1}, \tag{31}$$

where N is the norm of the wave function Ψ,

$$N = \int d\nu_1 d\nu_2 |\Psi(\nu_1,\nu_2)|^2, \tag{32}$$

and $\Psi(\nu_1,\nu_2)$ is given by Eq. (11).

In a general case, the integrals in Eqs. (31) and (32) cannot be calculated analytically, and even their numerical calculation is a rather difficult problem. To perform integrations we will use approximations following from the main features of the wave function (11) described above. Let us consider separately the cases of short and long pulses, $\eta \ll 1$ and $\eta \gg 1$.

A. Short pump pulses

The mismatch $\Delta(\nu_1,\nu_2)$ (8) entering the argument of the sinc function in the definition of $\Psi(\nu_1,\nu_2)$ is quadratic in ν_1. Hence the equation $\Delta=0$ has two solutions, $\nu_1^+(\nu_2)$ and $\nu_1^-(\nu_2)$. Only one of these solutions is compatible with the condition $|\nu_{1,2}| \ll \omega_0$, and this solution is given by an equation similar to Eq. (15),

$$\nu_1^-(\nu_2) \equiv f(\nu_2) = -\nu_2 + \frac{4B}{A\omega_0}\nu_2^2.$$

In the vicinity of ν_1^- the mismatch $\Delta(\nu_1,\nu_2)$ can be approximated by the linear function of ν_1,

$$\Delta \equiv \Delta(\nu_1,\nu_2) \approx \frac{A}{c}[\nu_1 - f(\nu_2)]. \tag{33}$$

The same approximation can be applied to all other functions Ψ in the definitions of the Schmidt number (31) and the norm of the wave function (32), which take then the form

$$K^{-1}N^2 = \int d\nu_1 d\nu_2 d\nu_1' d\nu_2' \exp\left[-\frac{(\nu_1+\nu_2)^2\tau^2}{8\ln 2}\right]\mathrm{sinc}\left[\frac{LA}{2c}[\nu_1 - f(\nu_2)]\right]\exp\left[-\frac{(\nu_1+\nu_2')^2\tau^2}{8\ln 2}\right]\mathrm{sinc}\left[\frac{LA}{2c}[\nu_1 - f(\nu_2')]\right] \times \exp\left[-\frac{(\nu_1'+\nu_2)^2\tau^2}{8\ln 2}\right]\mathrm{sinc}\left[\frac{LA}{2c}[\nu_1' - f(\nu_2)]\right]\exp\left[-\frac{(\nu_1'+\nu_2')^2\tau^2}{8\ln 2}\right]\mathrm{sinc}\left[\frac{LA}{2c}[\nu_1' - f(\nu_2')]\right] \tag{34}$$

and

$$N = \int d\nu_1 d\nu_2 \exp\left[-\frac{(\nu_1+\nu_2)^2\tau^2}{4\ln 2}\right]\left\{\mathrm{sinc}\left[\frac{LA}{2c}[\nu_1 - f(\nu_2)]\right]\right\}^2. \tag{35}$$

Still, the integrals (34) and (35) are too complicated for analytical calculation; but we can remember now that in the case of short pulses ($c\tau \ll AL/2$) the exponential functions in all integrals are much wider than the sinc functions. Hence, with a good accuracy, we can take off the exponential functions from the integrals at values of their arguments determined by the condition that the corresponding phase mismatch turns zero. With such a procedure applied to Eq. (35) we get

$$N = \frac{2\pi c}{LA}\int d\nu_2 \exp\left[-\frac{4B^2\nu_2^4\tau^2}{A^2\omega_0^2\ln 2}\right] = \frac{2^{3/2}\pi c}{L}(\ln 2)^{1/4}\Gamma\left(\frac{5}{4}\right)\sqrt{\frac{\omega_0}{AB\tau}}, \tag{36}$$

where we took into account that $\int_{-\infty}^{\infty}\mathrm{sinc}^2(x)dx = \pi$ and $\int_{-\infty}^{\infty} e^{-x^4}dx = 2\Gamma(5/4)$, Γ denotes the gamma function, and $\Gamma(5/4)=0.9064$.

For calculation of integrals in Eq. (34) we use the following exact equation for the integrated product of two sinc functions:

$$\int_{-\infty}^{\infty} dx\ \mathrm{sinc}(x)\mathrm{sinc}(x+y) = \pi\,\mathrm{sinc}(y). \tag{37}$$

Known or not, this equality can be easily proved, e.g., by means of analytical continuation to the complex plane x and integration by the residue method. With the help of the rule (37), we perform integration in Eq. (34) separately in the first and second pairs of lines under the symbol of integrals (correspondingly, over ν_1 and ν_1'), with the exponential functions taken out of the integrals, as explained above. As a result we get

$$K^{-1}N^2 = \left(\frac{2\pi c}{LA}\right)^2 \int d\nu_2 d\nu_2' \exp\left[-\frac{4B^2\tau^2}{A^2\omega_0^2 \ln 2}(\nu_2^4 + \nu_2'^4)\right] \times \left\{\mathrm{sinc}\left[\frac{LA}{2c}(\nu_2 - \nu_2')\right]\right\}^2. \quad (38)$$

Note that in the last expression the difference $\nu_1(\nu_2) - \nu_1(\nu_2')$ in the argument of the sinc function is approximated by $\nu_2' - \nu_2$, i.e., here the quadratic term of the expression in Eq. (15) is dropped both in $f(\nu_2)$ and $f(\nu_2')$. This is possible because in Eq. (38) the argument of the exponential function differs from that of the sinc function, and hence, small quadratic terms in the sinc-function argument are not needed for making integrals converging, as this was, e.g., in the case of integrations over ν_1 and ν_1'. The integrals in Eq. (38) are easily calculated with the help of the same procedure as used above, with the slow exponential function taken off from the integral over ν_2' at $\nu_2' = \nu_2$. The results are given by

$$K^{-1}N^2 = \left(\frac{2\pi c}{LA}\right)^3 \int d\nu_2 \exp\left[-\frac{8B^2\tau^2}{A^2\omega_0^2 \ln 2}\nu_2^4\right] = \left(\frac{2\pi c}{LA}\right)^3 \Gamma\left(\frac{5}{4}\right)(2\ln 2)^{1/4}\sqrt{\frac{A\omega_0}{B\tau}} \quad (39)$$

and

$$K_{\mathrm{short}} = \frac{N^2}{K^{-1}N^2} = \frac{(2\ln 2)^{1/4}}{\sqrt{\pi}}\Gamma\left(\frac{5}{4}\right)\frac{A^{3/2}}{\sqrt{B}}\frac{L}{\sqrt{c\tau\lambda_0}} = 0.785\frac{A}{\sqrt{B\eta}}\sqrt{\frac{L}{\lambda_0}} = \frac{57.5}{\sqrt{\eta}}. \quad (40)$$

Comparison with Eq. (20) shows that in the case of short pump pulses all functional dependences of R_{short} and K_{short} are identical and, numerically, the difference between R_{short} and K_{short} is very small, ~4.5%.

B. Long pulses

In the case of long pump pulses ($\eta \gg 1$) calculation of the Schmidt number is similar to that described above for short pulses, though the roles of the exponential (pump) and sinc functions are reversed: the pump spectral function is narrow and the sinc function is wide. Owing to this, the sinc function in Eq. (11) can be simplified in a way different from that used in Eqs. (33)–(35). In the case of long pulses the sum $\nu_1 + \nu_2$ is very small and the linear term in the argument of the sinc function can be dropped. As the result we can write down Eqs. (31) and (32) in the form

$$K^{-1}N^2 = \int d\nu_1 d\nu_2 d\nu_1' d\nu_2' \exp\left[-\frac{(\nu_1+\nu_2)^2\tau^2}{8\ln 2}\right]\mathrm{sinc}\left[\frac{LB}{2c}\frac{(\nu_1-\nu_2)^2}{\omega_0}\right]\exp\left[-\frac{(\nu_1+\nu_2')^2\tau^2}{8\ln 2}\right]\mathrm{sinc}\left[\frac{LB}{2c}\frac{(\nu_1-\nu_2')^2}{\omega_0}\right] \times \exp\left[-\frac{(\nu_1'+\nu_2)^2\tau^2}{8\ln 2}\right]\mathrm{sinc}\left[\frac{LB}{2c}\frac{(\nu_1'-\nu_2)^2}{\omega_0}\right]\exp\left[-\frac{(\nu_1'+\nu_2')^2\tau^2}{8\ln 2}\right]\mathrm{sinc}\left[\frac{LB}{2c}\frac{(\nu_1'-\nu_2')^2}{\omega_0}\right] \quad (41)$$

and

$$N = \int d\nu_1 d\nu_2 \exp\left[-\frac{(\nu_1+\nu_2)^2\tau^2}{4\ln 2}\right]\left\{\mathrm{sinc}\left[\frac{LB}{2c}\frac{(\nu_1-\nu_2)^2}{\omega_0}\right]\right\}^2. \quad (42)$$

The norm N is calculated easily with $\nu_2 = -\nu_1$ substituted into the argument of the wide sinc^2 function, after which the integral over ν_2 in Eq. (42) takes the Gaussian form to give

$$N = \frac{2\sqrt{\pi\ln 2}}{\tau}\int d\nu_1\left[\mathrm{sinc}\left(\frac{2LB\nu_1^2}{c\omega_0}\right)\right]^2 = \frac{2\sqrt{\pi\ln 2}}{\tau}\sqrt{\frac{c\omega_0}{2LB}}\frac{4\sqrt{\pi}}{3}, \quad (43)$$

where the last factor on the right-hand side of Eq. (43) arises from integration over the dimensionless variable $x = \nu_1\sqrt{2LB/c\omega_0}$: $\int_{-\infty}^{\infty} dx\ \mathrm{sinc}^2(x^2) = 4\sqrt{\pi}/3$.

The product of two exponential functions in the first and second lines under the symbol of integrals in Eq. (41) equals

$$\exp\left\{-\frac{\tau^2}{8\ln 2}[(\nu_1+\nu_2)^2 + (\nu_1+\nu_2')^2]\right\} = \exp\left\{-\frac{\tau^2}{4\ln 2}\left[\left(\nu_1 + \frac{\nu_2+\nu_2'}{2}\right)^2 + \frac{(\nu_2-\nu_2')^2}{4}\right]\right\}. \quad (44)$$

In dependence on ν_1 this narrow function has a maximum at $\nu_1 = -(\nu_2+\nu_2')/2$, and this is the value that has to be substituted instead of ν_1 into the wide sinc functions in the first and second lines under the symbol of integrals in Eq. (41). This substitution makes the sinc function independent of ν_1, and integration of the exponential function (44) over ν_1 is easily performed. Integration over ν_1' in the last two lines of Eq. (41) is performed exactly in the same way. Altogether, these

two integrations (over ν_1 and ν_1') reduce Eq. (41) to a simpler form,

$$K^{-1}N^2 = \frac{4\pi \ln 2}{\tau^2}\int d\nu_2 d\nu_2' \exp\left[-\frac{\tau^2}{8\ln 2}(\nu_2-\nu_2')^2\right] \times \mathrm{sinc}^2\left[\frac{LB}{8c\omega_0}(3\nu_2+\nu_2')^2\right]\mathrm{sinc}^2\left[\frac{LB}{8c\omega_0}(\nu_2+3\nu_2')^2\right], \tag{45}$$

where the first and second sinc^2 functions arise, correspondingly, from integration of the first and second pairs of lines in Eq. (41). In Eq. (45), again, the exponential function is narrow and sinc functions are wide in their dependence on, e.g., ν_2'. Owing to this, we can substitute ν_2' by ν_2 in the arguments of the sinc functions and take easily the arising Gaussian integral over ν_2' to get

$$K^{-1}N^2 = \frac{8\sqrt{2}(\pi\ln 2)^{3/2}}{\tau^3}\int d\nu_2\,\mathrm{sinc}^4\left(\frac{2LB\nu_2^2}{c\omega_0}\right) = \frac{8\sqrt{2}(\pi\ln 2)^{3/2}}{\tau^3}\sqrt{\frac{c\omega_0}{2LB}}\left[\frac{64}{105}(2^{3/2}-1)\sqrt{\pi}\right], \tag{46}$$

where the last factor in square brackets is the exact expression for the integral $\int_{-\infty}^{\infty}dx\,\mathrm{sinc}^4(x^2)$.

Equations (43) and (46) determine the Schmidt number in the long-pulse regime

$$K_{\mathrm{long}} = \frac{105\sqrt{\pi}}{72\sqrt{2\ln 2}(2^{3/2}-1)}\frac{c\tau}{\sqrt{BL\lambda_0}} = 0.6\frac{A\eta}{\sqrt{B}}\sqrt{\frac{L}{\lambda_0}} = 44\eta. \tag{47}$$

Comparison of this result with that of Eq. (26) shows that in the case of long pulses, as well as in the case of short pulses [Eqs. (20) and (40)], the Schmidt number and the parameter R are rather close to each other. Again, all functional dependences of Eqs. (47) and (26) are identical. The parameters K_{long} and R_{long} differ only by numerical coefficients. In the case of long pulses this difference is ~20%, i.e., somewhat larger than in the case of short pulses but, still, small enough to consider R as a good entanglement quantifier.

The Schmidt number for arbitrary pulse durations can be evaluated with the help of the same square-root interpolation as in the case of R [Eq. (29)]:

$$K(\eta) = \sqrt{K_{\mathrm{short}}^2 + K_{\mathrm{long}}^2} = \frac{A\eta}{\sqrt{B}}\sqrt{\frac{L}{\lambda_0}}\sqrt{\frac{(0.785)^2}{\eta}+(0.6\eta)^2} = \sqrt{\frac{(57.5)^2}{\eta}+(44\eta)^2}. \tag{48}$$

The function $K(\eta)$ is plotted in Fig. 4 (the dashed curve) together with $R(\eta)$. The difference between these two curves is more pronounced in the case of long pump pulses and is almost negligible in the case of short pulses; but even in the case of long pulses the parameters R and K are close enough to use the experimentally measurable parameter R as the entanglement quantifier.

The ratio of R and K parameters (29) and (48) equals

$$\frac{K(\eta)}{R(\eta)} \approx 1.04\sqrt{\frac{1+0.586\eta^3}{1+\eta^3}}. \tag{49}$$

Numerical coefficients on the right-hand side of this equation are not related to any parameters of the medium or pump and arise from $\ln 2$, $\sqrt{\pi}$, and similar factors. For this reason the ratio K/R can be considered as a universal function depending only on the control parameter η and valid for any crystals (with the type-I phase matching) and any pump wavelengths. Moreover, Eq. (49) and all other results derived above [except the very final numerical estimates in Eqs. (20), (21), (26), (40), (47), and (48)] can be applied to any processes generating bipartite states of the form (11) with arbitrary pairs of variables substituting ν_1 and ν_2 and with any values and physical origin of the constants A and B. In particular, the results described here can be applied directly to the earlier considered angular entanglement of SPDC biphoton states in a continuous pump laser [1]. Specifically, for establishing one-to-one correspondence between the spectral and angular entanglement, we have to substitute frequencies $\nu_{1,2}$ by angles $\theta_{1,2}$ determining directions of the photon wave vectors $\mathbf{k}_{1,2}$. In accordance with the approach of Ref. [1], we can consider the angular divergence of the pump α_0 as a varying parameter substituting in the case of a monochromatic pump the pump-pulse duration τ. Then, to reduce the angular wave function in the "parallel geometry" of Ref. [1] to the form of Eq. (11), we have to substitute the constants A [Eq. (9)] and B [Eq. (10)] and the control parameter η [Eq. (15)] by

$$\tilde{A} = \frac{\pi c}{\lambda_0}\frac{n_p'}{n_p}, \quad \tilde{A} = \frac{\pi^2c^2}{2n_p\lambda_0}, \quad \tilde{\eta} = \frac{4\ln 2\lambda_0}{\pi\alpha_0 L}\frac{n_p}{n_p'}, \tag{50}$$

where now n_p' is the angular derivative of the pump refractive index n_p. With these substitutions done, we can use all the results derived above for the Schmidt number K and the parameter R. In particular, with the help of Eq. (30) we can find the minimal value of the parameter R characterizing angular entanglement in the parallel geometry at varying angular divergence of the pump α_0:

$$R_{\mathrm{min}\parallel}^{\mathrm{angular}} = n_p'\sqrt{\frac{2L}{n_p\lambda_0}}. \tag{51}$$

This result was not obtained earlier in Ref. [1], and it shows that the degree of angular entanglement is high even in the most unfavorable circumstances owing to the same large factor as in the case of spectral entanglement, $\sqrt{L/\lambda_0} \gg 1$.

Note finally that in the analytical derivation of expressions (40) and (47) for the Schmidt number in the short- and long-pulse limits we used approximations, precision of which was not controlled and, probably, could not be controlled analytically. Hence exact numerical calculations of the Schmidt number $K(\tau)$ are needed for making the final conclusion on how close are $K(\tau)$ and $R(\tau)$. Such calculations were done recently by Mauerer and Silberhorn [18]. They show that "$K_{\mathrm{exact}}(\tau)$" and $R(\tau)$ are even closer to each other than predicted by analytical calculations. Coincidence of $K_{\mathrm{exact}}(\tau)$ and $R(\tau)$ is almost perfect in the limits of short

and long pump pulses. The largest discrepancy occurs in the intermediate region around minima of the curves "$K_{\text{exact}}(\tau)$" and $R(\tau)$; but even in this region the discrepancy is only about 10%. This shows that for the wave function of the form (11) the Schmidt number K and R parameter are really close to each other and that even the used above simple interpolation formula (28) gives a pretty good result.

VI. TEMPORAL STRUCTURE OF BIPHOTON WAVE PACKETS

A. General expression

Temporal and coordinate features of biphoton states are characterized by the function $\tilde{\Psi}(t_1,t_2;z_1,z_2)$ depending on two times t_1 and t_2 and two coordinates, z_1 and z_2,

$$\tilde{\Psi}(t_1,t_2;z_1,z_2) = \int d\omega_1 d\omega_2 \Psi(\omega_1,\omega_2) \times \exp\{-i[\omega_1 t_1 - k_1(\omega_1)z_1 + \omega_2 t_2 - k_2(\omega_2)z_2]\}. \quad (52)$$

The wave function $\tilde{\Psi}$ determines the probability density

$$\frac{dw}{dt_1 dz_1 dt_2 dz_2} = |\tilde{\Psi}(t_1,t_2;z_1,z_2)|^2 \quad (53)$$

of finding (registering) photons "1" and "2" in small vicinities of arbitrary points (z_1,t_1) and (z_2,t_2) in the coordinate-time plane (z,t) under the condition that z_1 and z_2 are within the crystal, i.e., $0 \leqslant z_{1,2} \leqslant L$.

The exponential factors depending on (z_1,t_1) and (z_2,t_2) on the right-hand side of Eq. (52) are the time-coordinate wave functions of one-photon states with momenta k_1 and k_2 (or frequencies ω_1 and ω_2),

$$e^{i(\omega_1 t_1 - k_1 z_1)} = \langle z_1,t_1|k_1\rangle = \langle z_1,t_1|a_{k_1}^{\dagger}|\text{vac}\rangle,$$

$$e^{i(\omega_2 t_2 - k_2 z_2)} = \langle z_2,t_2|k_2\rangle = \langle z_2,t_2|a_{k_2}^{\dagger}|\text{vac}\rangle. \quad (54)$$

The two-time and two-coordinate wave function of Eq. (52) is the projection of the two-photon state vector given by the second term on the right-hand side of Eq. (1) upon the product of two coordinate states,

$$\tilde{\Psi}(t_1,t_2;z_1,z_2) = \langle z_1,t_1|\langle z_2,t_2| \sum_{\mathbf{k_1},\mathbf{k_2}} \Psi(\mathbf{k_1},\mathbf{k_2})|\mathbf{k_1},\mathbf{k_2}\rangle, \quad (55)$$

for the case $\mathbf{k}_{1,2\perp}=0$.

Note that owing to the presence of coordinate parts in these single-photon wave functions, the transition from spectral to temporal picture determined by Eq. (52) is not equivalent to the simple double Fourier transform of $\Psi(\omega_1,\omega_2)$ used in Refs. [9,19]. Though some results of these two types of calculations can coincide [see Eq. (61) and explanations below], in a general case, transition to the temporal picture is inseparable from transition to the coordinate representation, and this is the transformation determined by Eq. (52) that gives a rigorously defined two-time and two-coordinate biphoton wave function.

As it was done previously, the wave vectors $k_{1,2}(\omega_{1,2})$ in Eq. (52) can be expanded in powers of small differences $\nu_{1,2}=\omega_{1,2}-\frac{1}{2}\omega_0$, with only the first and second orders to be retained,

$$k_{1,2}(\omega_{1,2}) \approx \frac{\omega_0}{2c} + \frac{\nu_{1,2}}{v_g^{(o)}} + \frac{2B}{c\omega_0}\nu_{1,2}^2 + \cdots. \quad (56)$$

By using this expansion, the definition of Eq. (52), and the expression of Eq. (5) for the frequency-dependent wave function $\Psi(\omega_1,\omega_2)$, we get the following integral representation for $\tilde{\Psi}$:

$$\tilde{\Psi}(t_1,t_2;z_1,z_2) \propto \int_0^L dz \int d\nu_1 d\nu_2 \exp\left[-\frac{(\nu_1+\nu_2)^2\tau^2}{8\ln 2}\right]\exp\left[-i\nu_1\left(t_1-\frac{z_1}{v_g^{(o)}}\right)-i\nu_2\left(t_2-\frac{z_2}{v_g^{(o)}}\right)+i\frac{Az}{c}(\nu_1+\nu_2)\right] \times \exp\left[i\frac{B}{c\omega_0}\left(z-\frac{z_1+z_2}{2}\right)(\nu_1-\nu_2)^2\right], \quad (57)$$

where, as previously stated, the squared frequencies $\nu_{1,2}^2=\frac{1}{4}[\nu_1-\nu_2\pm(\nu_1+\nu_2)]^2$ in the expansion (56) are approximated by $\frac{1}{4}(\nu_1-\nu_2)^2$ with the terms $\pm\frac{1}{2}(\nu_1-\nu_2)(\nu_1+\nu_2)$ and $\frac{1}{4}(\nu_1+\nu_2)^2$ dropped as giving only small corrections to other terms $\propto\nu_1+\nu_2$ and $\propto(\nu_1-\nu_2)^2$ in the exponential functions of Eq. (57).

In variables $u=\nu_1+\nu_2$ and $v=\nu_1-\nu_2$ the double integral over ν_1 and ν_2 in Eq. (57) splits for the product of two Gaussian integrals over u and v which are easily taken to give

$$\tilde{\Psi}(t_1,t_2;z_1,z_2) \propto \int_0^{\min(z_1,z_2)} \frac{dz}{\sqrt{\frac{z_1+z_2}{2}-z}} \exp\left\{-\frac{2\ln 2}{c^2\tau^2}\left[Az-\frac{c(t_1+t_2)}{2}+\frac{c(z_1+z_2)}{2v_g^{(o)}}\right]^2\right\} \times \exp\left\{\frac{i\pi c^2}{4B\lambda_0(z_1+z_2-2z)}\left(t_1-t_2-\frac{z_1-z_2}{v_g^{(o)}}\right)^2\right\}. \quad (58)$$

Here we restricted the region of integration over z by $\frac{1}{2}(z_1+z_2)$ (instead of L) because we interpret z as the coordinate of birth of a single-idler pair, and z_1 and z_2 as possible locations of the emitted photons. As these photons propagate to the direction of growing $z_{1,2}$, these coordinates cannot be smaller than the coordinate of their birth, i.e., z must be smaller than $\min\{z_1,z_2\}$.

At the exit from the crystal, where $z_1=z_2=L$, Eq. (58) takes the form

$$\tilde{\Psi}(t_1,t_2) \equiv \tilde{\Psi}(t_1,L;t_2,L) \propto \int_0^L \frac{dz}{\sqrt{L-z}} \times \exp\left\{-\frac{2\ln 2}{\tau^2}\left[\frac{z}{v_g^{(e)}}+\frac{(L-z)}{v_g^{(o)}}-\frac{(t_1+t_2)}{2}\right]^2\right\} \times \exp\left\{i\frac{\pi c^2}{8B\lambda_0(L-z)}(t_1-t_2)^2\right\}. \quad (59)$$

Finally, by introducing new time variables

$$\tilde{t}_{1,2} = t_{1,2} - \frac{L}{v_g^{(o)}}, \quad t_+ = \frac{1}{2}(\tilde{t}_1+\tilde{t}_2), \quad t_- = \tilde{t}_1-\tilde{t}_2, \quad (60)$$

we can slightly simplify the first exponential factor on the right-hand side of Eq. (59) and get

$$\tilde{\Psi}(\tilde{t}_1,\tilde{t}_2) \propto \int_0^L \frac{dz}{\sqrt{L-z}} \times \exp\left\{-\frac{2\ln 2}{c^2\tau^2}(Az-ct_+)^2\right\}\exp\left\{i\frac{\pi c^2 t_-^2}{8B\lambda_0(L-z)}\right\}. \quad (61)$$

The time shift $L/v_g^{(o)}$ in Eq. (60) is the time during which the signal and idler photons moving exactly with their group velocity cross all of the crystal from 0 to L. Hence if $t_1=t_2=0$ is the time when the peak of the temporal envelope of the pump enters the crystal, the zero point for $\tilde{t}_{1,2}$ ($\tilde{t}_{1,2}=0$) is the time when the signal and idler photons, emitted at $t_1=t_2=0$ and moving with the speed $v_g^{(o)}$, reach the end of the crystal.

Note that substitution of the integration variable $z=z'+L$ and some additional shift of the time variables $\tilde{t}_1$ and $\tilde{t}_2$ reduce Eq. (61) to the same form as that of Eq. (22) in the paper by Keller and Rubin [9]. This equation of Ref. [9] was obtained with the help of a simple double Fourier transformation rather than via the transition from momentum to time-coordinate representation determined by Eq. (52). Though seemingly surprising, this coincidence is quite understandable. Indeed, in terms of z', the crystal borders are $-L$ and 0, and at the exit from the crystal $z_1'=z_2'=0$. At this point, the one-photon wave functions of Eq. (54) (with z substituted by z') turn into $e^{-i\omega_{1,2}t_{1,2}}$, and the transformation of Eq. (52) appears to be equivalent to the double Fourier transformation. However, this is a very exceptional case related to the assumed in Ref. [9] location of the crystal at $(-L,0)$. Our attempt [19] to apply a simple double Fourier transformation to the case when the crystal location is taken as $(0,L)$ gave a result qualitatively different from that of Eq. (61) and, evidently, wrong. Here in Eq. (61) we correct it with the help of derivation based on the transformation from the frequency to time-coordinate representation of Eq. (52).

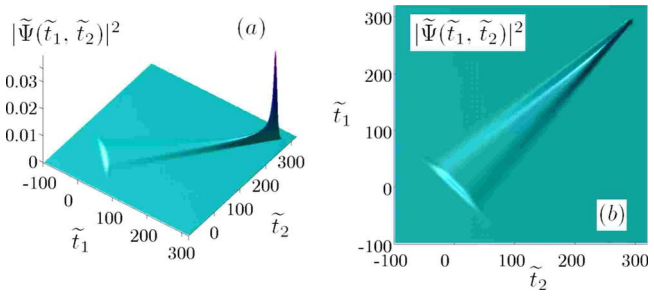

FIG. 5. (Color online) The function $|\tilde{\Psi}(\tilde{t}_1,\tilde{t}_2)|^2$ (in relative units) for $\tau=50$ fs, (a) 3D plot and (b) the top view; $\tilde{t}_1$ and $\tilde{t}_2$ are in units of 10 fs.

Actually, the results of calculations have to be invariant with respect to the choice of coordinates determining the location of the crystal. We can easily find that the transformation determined by Eq. (52) provides such invariance whereas the simple double Fourier transformation does not. Indeed, the difference between Eqs. (61) and (10) of Ref. [19] is in a different location of the singularity in the integral over z: at $z=L$ (the exit edge of a crystal) in Eq. (61) and $z=0$ (the entrance edge) in Eq. (10) of Ref. [19]. Location of the singularity is determined by the factor in front of $(\nu_1-\nu_2)^2$ in the last line of Eq. (57) and in similar equations of Refs. [9,19]. Let in a general case the coordinates of the crystal edges be $z=L_1$ and $z=L_2=L_1+L$. We are interested in the biphoton wave function at the exit edge, i.e., $z_1=z_2=L_2$. In this case, the coefficient in front of $(\nu_1-\nu_2)^2$ in the last line of Eq. (57) is proportional to $z-L_2$, and the singularity in the final integral over z [similar to that of Eq. (61)] occurs at $z=L_2$, i.e., always at the exit edge of the crystal. In contrast to this, in the scheme of calculation with the double-Fourier transformation the coefficient in front of $(\nu_1-\nu_2)^2$ in the last line of Eq. (57) becomes proportional to z, i.e., the singularity in the final integral over z occurs at $z=0$. This point can be arbitrarily located with respect to the crystal and, evidently, the results are not invariant with respect to the choice of the crystal coordinates. The only case when the results of calculations in these two approaches coincide is the case $L_1=-L$ and $L_2=0$, and this is just the case of Ref. [9].

B. Numerical results

1. Short pump pulses

The probability density of registering photons at the exit from the crystal at times $\tilde{t}_1$ and $\tilde{t}_2$ is given by the squared absolute value of the wave function $\tilde{\Psi}(\tilde{t}_1,\tilde{t}_2)$ (61), determining a surface in the three-dimensional (3D) space $\{\tilde{t}_1,\tilde{t}_2,|\tilde{\Psi}|^2\}$. For short pump pulses $\tau=50$ fs and for the same values of all other parameters which were used above, the surface $\tilde{\Psi}(\tilde{t}_1,\tilde{t}_2)$ is shown in Fig. 5.

The surface $|\tilde{\Psi}(\tilde{t}_1,\tilde{t}_2)|^2$ is seen to have the form of a long plateau symmetric in t_1, t_2. The plateau is rather wide in the beginning (at small values $\tilde{t}_{1,2}$) and is narrowing and height-

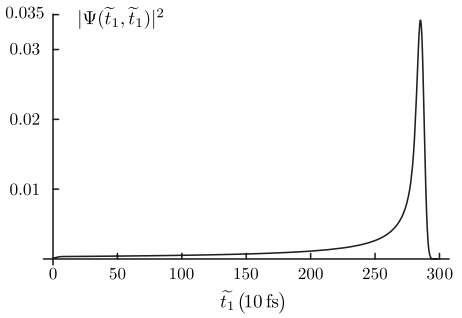

FIG. 6. The diagonal squared wave function $|\tilde{\Psi}(\tilde{t}_1,\tilde{t}_1)|^2$ (in relative units).

ening with a growing value of $\tilde{t}_1+\tilde{t}_2$. Around the point $\tilde{t}_1=\tilde{t}_2=285.25$ the plateau turns into a rather high and sharp peak. The diagonal squared wave function $|\tilde{\Psi}(\tilde{t}_1,\tilde{t}_1)|^2$ characterizes evolution of the plateau-peak height in its dependence on $\tilde{t}_1+\tilde{t}_2$, and this function is shown in Fig. 6. In accordance with the 3D picture of Fig. 5(a), the curve of Fig. 6 switches on rather quickly at $t=0$ (in a time on the order of the pulse duration of the pump τ), and then it has a long and slowly growing plateau ending with a high and narrow peak at $t=2.8525$ ps followed by a very quick turn-off.

The temporal shape and parameters of coincidence and single-particle signals are defined in the same way as in the cases of frequency or angular distributions. The coincidence signal is determined by the probability density $dw^{(c)}(t_1)/dt_1$ of registering at the exit surface of the crystal a photon "1" at a varying time $\tilde{t}_1$ under the condition that the photon "2" of the same pair is registered at the same place at some given time $\tilde{t}_2$, $dw^{(c)}(t_1)/dt_1 \propto |\tilde{\Psi}(\tilde{t}_1,\tilde{t}_2)|^2$ at $\tilde{t}_2=$const. For 50-fs pulses of the pump, two examples of coincidence curves are shown in Fig. 7.

These curves correspond to the very beginning of the plateau and to the peak of the surface $|\tilde{\Psi}(\tilde{t}_1,\tilde{t}_2)|^2$ in Fig. 5. The FWHM of the curves (a) and (b) in Fig. 7 are equal to $\Delta t_1^{(c)}(\tilde{t}_2=0)=486.3$ fs and $\Delta t_1^{(c)}(\tilde{t}_2=2.8525\ \text{ps})=6$ fs. This huge difference in FWHM shows clearly that in the temporal picture the coincidence widths $\Delta t_1^{(c)}$ (or the duration of the coincidence signal) depends very strongly on the registration time t_2 of the second photon of a pair. This contrasts with the spectral picture where $\Delta\nu_1^{(c)}$ was shown to be almost independent of ν_2. A strong dependence of $\Delta t_1^{(c)}$ on t_2 makes the temporal picture inappropriate for defining the parameter R and for determining in such a way the degree of entanglement. Such a procedure can be used only in the spectral

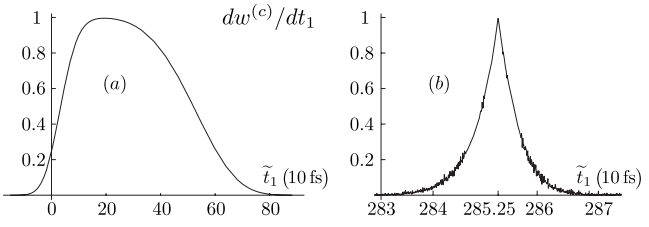

FIG. 7. Normalized coincidence signals at (a) $\tilde{t}_2=0$ and (b) $\tilde{t}_2=2.8525$ ps.

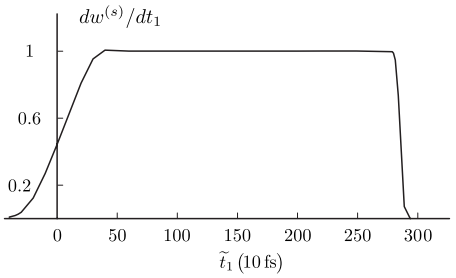

FIG. 8. The normalized time-dependent single-particle probability density; $\tilde{t}_1$ and $\tilde{t}_2$ are in units of 10 fs.

picture. Some analogies can be found in the coordinate and momentum pictures for massive particles, where spreading of wave packets in the coordinate representation makes the latter inconvenient for evaluation of the degree of entanglement via the width-ratio parameter R; whereas the momentum representation is free from such a problem because momentum distributions do not spread [4]. In the case of photons, dispersion (or diffraction divergency) plays the role analogous to spreading.

The single-particle temporal density of probability to register a photon by a single detector at a varying time t_1 is determined by the integrated squared two-time wave function of Eq. (61),

$$\frac{dw^{(s)}(t_1)}{dt_1} \propto \int dt_2 |\tilde{\Psi}(t_1,t_2)|^2. \tag{62}$$

For the pump-pulse duration as short as $\tau=50$ fs the result of numerical integration is plotted in Fig. 8. Duration of the single-particle signal, defined as FWHM of the curve in Fig. 8, equals 2.837 ps, which is more than 50 times longer than the pump pulse.

Two other interesting features of the curve $dw^{(s)}(t_1)/dt_1$ are its constant value at a very long interval of time and the anomalously long front wing (at small $\tilde{t}_1$). Explanations are given below in Sec. VI C on the basis of simplified analytical formulas.

2. Long pump pulses

All the results shown in Figs. 5–8 correspond to a short duration of the pump pulses ($\eta \ll 1$). In the case of long pulses ($\eta \gg 1$) the picture changes rather significantly. For $\tau=2$ ps the 3D pictures of Fig. 5 are substituted by those of Fig. 9.

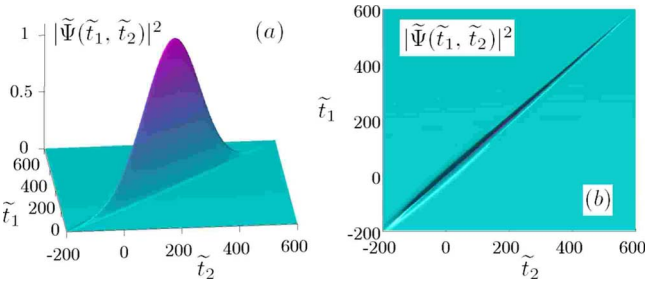

FIG. 9. (Color online) The same as in Fig. 5 but for $\tau=2$.

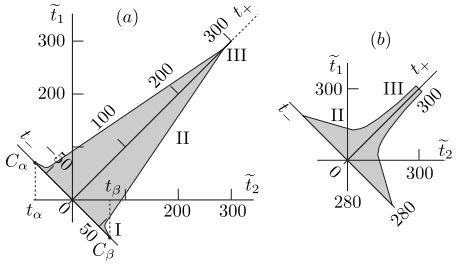

FIG. 10. Localization region of the function $\tilde{\Psi}(\tilde{t}_1,\tilde{t}_2)$; $\tilde{t}_1$, $\tilde{t}_2$, t_+, and t_- are in units of 10 fs; (b) is the increased section III of (a).

The surface $\tilde{\Psi}(\tilde{t}_1,\tilde{t}_2)$ is seen to have the form of a narrow long bump concentrated along the diagonal $\tilde{t}_1=\tilde{t}_2$ in the plane $(\tilde{t}_1,\tilde{t}_2)$. As seen clearly in Fig. 10(b), the width of the layer $\tilde{\Psi}(\tilde{t}_1,\tilde{t}_2)$ is almost constant in the middle part of the bump, and the layer narrows slightly at its ends. Quantitative characteristics of the temporal photon distribution are presented below in Sec. VI D.

C. Analytical characterization for short pump pulses

1. Simplified formulas

If the pump pulses are short enough, $c\tau \ll AL$, the first exponential factor in the integrand of Eq. (61) is very narrow. Location of its peak determines the coordinate $z_0=ct_+/A$, a small vicinity of which gives the main contribution to the integral over z. Under these conditions we can simplify the integrand by substituting $z=z_0$ into the preexponential factor $1/\sqrt{L-z}$ and by expanding $1/(L-z)$ in the second exponential factor in powers of $|z-z_0|/z_0$: $1/(L-z)\approx 1/(L-z_0)+(z-z_0)/(L-z_0)^2$. As a result of such simplifications, the integral in Eq. (61) takes the Gaussian form with finite limits of integration, which gives rise to the sum of two error functions:

$$\tilde{\Psi}(t_+,t_-) \propto \frac{1}{\sqrt{LA-ct_+}} \exp\left[-a^2\left(\frac{ct_-}{LA-ct_+}\right)^4\right] \times\left\{\operatorname{erf}\left[\sqrt{2\ln 2}\frac{AL-ct_+}{c\tau}+ia\left(\frac{ct_-}{AL-ct_+}\right)^2\right] - \operatorname{erf}\left[-\sqrt{2\ln 2}\frac{t_+}{\tau}+ia\left(\frac{ct_-}{LA-ct_+}\right)^2\right]\right\}, \quad (63)$$

where

$$a=\frac{\pi c\tau A}{16\sqrt{2\ln 2}B\lambda_0}. \quad (64)$$

The validity criterion of the approximation used for derivation of Eq. (63) is $|z-z_0| \ll L-z_0$ with $z_0=ct_+/A$ and $|z-z_0| \sim c\tau/A$, which gives

$$LA-ct_+ \gg c\tau. \quad (65)$$

As t_+ is associated with the location z_0 of the peak of the pump envelope in the crystal, the condition (65) means that the pump pulse is located far enough from the end of the crystal, at a distance exceeding significantly $c\tau/A$. Note that the times $t_+=0$ and $t_+=LA/c$ are associated with the pump pulse entry to and exit from the crystal.

If, in addition to Eq. (65), the time t_+ or coordinate z_0 obey the conditions $t_+ \gg \tau$ or $z_0 \gg c\tau/A$, the pump envelope is located far from both edges of the crystal. In this case the formula of Eq. (66) can be further significantly simplified. Indeed, if a very short pump pulse is located deep in the crystal, the limits of integration over z can be extended to $-\infty$ and $+\infty$. This is equivalent to approximation of the first and second error functions in Eq. (63) by +1 and −1, and reduces finally Eq. (63) to the simplest form:

$$\tilde{\Psi}(t_+,t_-) \propto \frac{1}{\sqrt{LA-ct_+}} \exp\left[-a^2\left(\frac{ct_-}{LA-ct_+}\right)^4\right]. \quad (66)$$

Equations (63) and (66) are much more convenient than the exact formula (61) for obtaining analytical expressions for parameters characterizing coincidence and single-particle signals.

2. Localization of the temporal biphoton wave packet

The localization region of the wave function $\tilde{\Psi}(\tilde{t}_1,\tilde{t}_2)$ in the $(\tilde{t}_1,\tilde{t}_2)$ plane can be defined in the following way: we plot graphs of $|\tilde{\Psi}|^2$ as a function of t_- at all given values of t_+ and find coordinates $t_-^{\pm}(t_+)$ of these curves at half-maxima. Then the functions $t_-^{\pm}(t_+)$ together with the line $t_+=0$ determine the borders of the localization region of $|\tilde{\Psi}(\tilde{t}_1,\tilde{t}_2)|^2$. With the functions $t_-^{\pm}(t_+)$ calculated numerically from Eq. (61) the result is given by the diagram of Fig. 10, in which $t_-^{+}(t_+)$ and $t_-^{-}(t_+)$ determine the upper and lower borders of the shaded area. Defined in such a way, the diagram of Fig. 10 agrees perfectly with the top view of the surface $|\tilde{\Psi}(\tilde{t}_1,\tilde{t}_2)|^2$ in Fig. 5(b). In Fig. 10 one can distinguish clearly three regions of t_+, I, II, and III, in which the dependence $t_-^{\pm}(t_+)$ is significantly different. Below these regions are analyzed separately.

3. Coincidence width in the region II

The most extended of the three regions in Fig. 10 is the region of intermediate values of t_+, II, where the wave function $\tilde{\Psi}(t_+,t_-)$ can be satisfactorily approximated by the simplest exponential formula of Eq. (66). This equation gives

$$t_-^{\pm}(t_+) = \pm\frac{4}{c}\sqrt{\frac{\ln 2AB\lambda_0}{\pi Ac\tau}}(LA-ct_+). \quad (67)$$

By definition, Eq. (67) determines the upper and lower boundaries of the localization region in Fig. 10 at a given value of t_+. However, the same equation can be used to find the upper and lower boundaries of the localization region $\tilde{t}_1^{\pm}$ at a given $\tilde{t}_2$. To find $\tilde{t}_1^{\pm}(\tilde{t}_2)$ one has to make a substitution in Eq. (67), $t_+=\frac{1}{2}(\tilde{t}_1+\tilde{t}_2)$, to replace $\tilde{t}_-^{\pm}$ by $\tilde{t}_1-\tilde{t}_2$, and to solve the arising equation with respect to $\tilde{t}_1$. In the first order in a small parameter $2\sqrt{\ln 2B\lambda_0/\pi c\tau}\approx 0.1 \ll 1$ (at $\tau=50$ fs) the solution is given by

$$\tilde{t}_1^{\pm}(\tilde{t}_2) = \tilde{t}_2\left(1 \mp 4\sqrt{\frac{\ln 2B\lambda_0}{\pi A c\tau}}\right) \pm \frac{4L}{c}\sqrt{\frac{\ln 2AB\lambda_0}{\pi c\tau}}. \quad (68)$$

From this equation we obtain the following analytical expression for the width of the coincidence temporal distribution of photons in the region II of Fig. 10:

$$\Delta t_1^{(c)}(\tilde{t}_2) = \tilde{t}_1^{+} - \tilde{t}_1^{-} = \frac{8}{c}\sqrt{\frac{B\lambda_0 \ln 2}{\pi A c\tau}}(LA - c\tilde{t}_2). \quad (69)$$

This expression shows that for photons coming in pairs to the exit from the crystal, their spread in the arrival time their is determined by a joint influence of the temporal walk-off and dispersion. The spread is large at small values of the observation time (small $\tilde{t}_2$) and falls with a growing $\tilde{t}_2$. This dependence of $\Delta t_1^{(c)}(\tilde{t}_2)$ on the observation time $\tilde{t}_2$ has a very clear qualitative explanation. Dispersion of velocities acquired by photons of a pair at their birth gives rise to retardation of one photon with respect to another during their propagation in a crystal. This retardation grows with the length of propagation. For photons born at the crystal entrance ($\tilde{t}_2 \approx 0$), both the propagation length and retardation are very large which results in a long duration of the coincidence signal [the picture of Fig. 7(a)]. For photons born close to the crystal exit ($\tilde{t}_2 \approx 0 \sim L/v_g^{(0)}$), the length of propagation is almost zero, and the resulting retardation and duration of the coincidence signal are very small [Fig. 7(b)].

4. Region I

In region I the simplest approximate formula of Eq. (66) is invalid; but the formula of Eq. (63) works perfectly and can be used to find analytical expressions determining both the shape of boundaries of localization region in Fig. 10 and the coincidence width of the temporal distribution of photons. As in region I the time t_+ is very small, the first error function in Eq. (63) equals unity, and the term t_+ can be dropped everywhere except the first term in the argument of the second error function to give

$$\tilde{\Psi} \propto e^{-y^4}[1 + \mathrm{erf}(b + iy^2)], \quad (70)$$

where $b = \sqrt{2\ln 2}t_+\tau$, $y = ct_-\sqrt{a}/LA$, and a is defined in Eq. (64). From Eq. (70) we find easily (e.g., with the help of simple calculation in Mathematica) that at $b=0$ the half-width at the half-maximum (HWHM) of $|\tilde{\Psi}|^2$ equals one, and at growing but small values of b it falls as $1-0.24b$. In terms of t_+ and t_- this yields

$$t_-^{\pm}(t_+) = \pm\frac{LA}{c\sqrt{a}}\left(1 - 0.24\frac{\sqrt{2\ln 2}t_+}{\tau}\right) = \frac{4L(2\ln 2)^{1/4}\sqrt{AB\lambda_0}}{c\sqrt{\pi c\tau}}\left(1 - 0.24\frac{\sqrt{2\ln 2}t_+}{\tau}\right). \quad (71)$$

The lines $t_-^{\pm}(t_+)$ determined by Eq. (71) are sharper than the lines determined by Eq. (67). The crossing points of these lines occur at $t_+ \approx 43$ fs and they determine the boundary between the zones I and II in Fig. 10. As seen well in Fig. 10, the width of the localization region in the t_- direction is maximal at $t_+=0$ where, in accordance with Eq. (71), it equals

$$\Delta t_{-\max} = t_-^{+}(t_+=0) - t_-^{-}(t_+=0) = \frac{8L(2\ln 2)^{1/4}\sqrt{AB\lambda_0}}{c\sqrt{\pi c\tau}} \approx 1.46 \text{ ps}. \quad (72)$$

5. Pulse shape of a single-particle signal

A large width of the wave-packet localization region in the t_- direction at $t_+=0$ explains the origin and parameters of the anomalously long front wing of the single-particle signal shown in Fig. 8. Indeed, owing to the condition $t_+=0$, in the $(\tilde{t}_1,\tilde{t}_2)$ frame the points C_α and C_β in Fig. 10 have coordinates $\tilde{t}_{1\alpha} = -\tilde{t}_{2\alpha} = \frac{1}{2}\Delta t_{-\max}$ and $\tilde{t}_{1\beta} = -\tilde{t}_{2\beta} = -\frac{1}{2}\Delta t_{-\max}$, where $\Delta t_{-\max}$ is given by Eq. (72). As the t_1-dependent single-particle signal can be considered as the sum of all coincidence signals at all values of t_2, it is clear that at $\tilde{t}_2 < \tilde{t}_{2\alpha}$ there are no signals at all, either in coincidence or single-particle measurements. Hence $\tilde{t}_{2\alpha}$ is that time since which the single-particle signal become detectable. Actually, $\tilde{t}_{2\alpha}$ is the beginning of the transient period during which the amplitude of the single-particle grows. This transient period ends at $\tilde{t}_2 = \tilde{t}_{2\beta}$, and its duration equals $\Delta t_{-\max}$ [Eq. (72)]. The same value characterizes the duration τ_{fw} of the front wing of the single particle signal considered as a function of t_1:

$$\tau_{\mathrm{fw}} = \tilde{t}_{1\alpha} - \tilde{t}_{1\beta} = \frac{8L(2\ln 2)^{1/4}\sqrt{AB\lambda_0}}{c\sqrt{\pi c\tau}}. \quad (73)$$

As is seen from Fig. 8, the single-particle signal is constant for all its duration after ending of the initial transient period. This feature is easily explained by Eqs. (66) and (69). Indeed, at a given $\tilde{t}_1$ the single-particle yield (62) can be estimated approximately as the product of the height $|\tilde{\Psi}(\tilde{t}_1,\tilde{t}_1)|^2$ and width $\Delta t_2^{(c)}(\tilde{t}_1)$ of $|\tilde{\Psi}\ \tilde{t}_1,\tilde{t}_2)|^2$ considered as a function $\tilde{t}_2$. The first of these two factors is given by Eq. (66) with $t_-=0$ and, evidently, $|\tilde{\Psi}(\tilde{t}_1,\tilde{t}_1)|^2 \propto 1/(LA - c\tilde{t}_1)$. As for the width $\Delta t_2^{(c)}(\tilde{t}_1)$, it is given by Eq. (69) with $\tilde{t}_2$ on its right-hand side substituted by $\tilde{t}_1$, and this gives $\Delta t_2^{(c)}(\tilde{t}_1) \propto LA - c\tilde{t}_1$. Hence with a growing $\tilde{t}_1$ the peak height of the function $|\tilde{\Psi}(\tilde{t}_1,\tilde{t}_2)|^2$ (in its dependence on $\tilde{t}_2$) grows, whereas its width falls, but their product remains constant (independent of $\tilde{t}_1$), i.e., the dependence $dw^{(s)}(\tilde{t}_1)/d\tilde{t}_1$ has the form of a plateau.

The total duration of the single-particle signal is determined by the condition that the real part of the argument of the second error function in Eq. (63) changes its sign, i.e.,

$$\tau_{\mathrm{single}} \approx \frac{LA}{c} = \frac{L}{v_g^{(e)}} - \frac{L}{v_g^{(o)}}. \quad (74)$$

This result is absolutely understandable qualitatively: τ_{single} is the period of time between the arrival and exit from the crystal of almost first and almost last observable SPDC photons or the delay time between the arrival of the first ordinary-wave photons and of the pump (extraordinary wave).

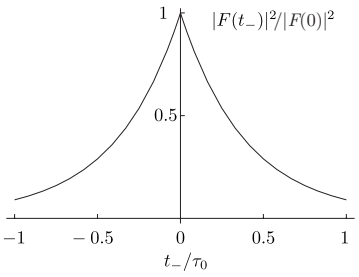

FIG. 11. Squared absolute value of the expression on the right-hand side of Eq. (82).

Note that qualitatively the long-plateau shape of the single-particle temporal signal was forecasted earlier [20]. In our analysis we specify quantitatively parameters of the plateau and, in addition, we describe such a striking feature of the single-particle signal as its unusually long front wing.

6. Region III in the diagram of Fig. 10

This is the region behind the peak of the photon distribution in Fig. 5(a), where the amount of photons is vary small. Nevertheless, this region is interesting because here formation of the localization region of the temporal wave packet is related to a mechanism qualitatively different from those described above for regions I and II. In region III the condition of Eq. (65) is not fulfilled, the fraction $1/(L-z)$ in the integrand of Eq. (61) cannot be expanded in powers of $(z-z_0)/(L-z_0)$, and the simple formulas of Eqs. (63) and (66) are invalid; but some estimates can be done directly on the ground of Eq. (61). Indeed, from the second exponential factor in the integrand on the right-hand side of Eq. (61) we can deduce the following estimate of the characteristic half-width of the wave-packet localization region

$$\Delta t_{\pm} \sim \pm \frac{\sqrt{B\lambda_0(L-z)}}{c}. \tag{75}$$

If the peak of the laser pulse is located exactly at the end of the crystal, $ct_+ = LA$, then the maximal deviation of z from L, where the integrand of Eq. (61) is not small, is $L-z \sim c\tau/A$. Substitution of this expression into Eq. (75) gives

$$\Delta t_-^{\pm} \sim \pm \frac{\sqrt{B\lambda_0\tau}}{\sqrt{cA}}. \tag{76}$$

This expression corresponds to the very beginning of zone III in Fig. 10.

If $ct_+ > L$, the peak of the pump pulse is located behind the crystal and only a small part if its rear wing remains in the crystal. By expanding the Gaussian exponent in powers of $L-z$, we find that now $L-z \sim c^2\tau^2/[A(ct_+ - LA)]$. By substituting this expression into Eq. (75), we find the law by which zone III in Fig. 10 slowly narrows,

$$\Delta t_-^{\pm} \sim \pm \tau \sqrt{\frac{B\lambda_0}{A(ct_+ - L)}}. \tag{77}$$

D. Long pump pulses: Analytical description and degree of entanglement

The regime of long pulses of the pump arises if the pulse duration is so long that $\tau \gg LA/c$ or $\eta \gg 1$ where η is given by Eq. (14). In this case the term proportional to z can be dropped in the argument of the first exponential function in Eq. (61) to give

$$\tilde{\Psi}(\tilde{t}_1, \tilde{t}_2) \propto \exp\left[-2\ln 2\left(\frac{t_+}{\tau}\right)^2\right] F(t_-), \tag{78}$$

where

$$F(t_-) = \int_0^L \frac{dz}{\sqrt{L-z}} \exp\left[i\frac{\pi c^2 t_-^2}{8B\lambda_0(L-z)}\right]. \tag{79}$$

Equation (78) shows that for long pulses the dependences of the wave function $\tilde{\Psi}$ on t_+ and t_- are factorized, and the dependence of $\tilde{\Psi}$ on t_+ repeats the time-dependence of the pump envelope. As for the integral over z in Eq. (79) determining the dependence of $\tilde{\Psi}$ on t_-, it can be calculated to expressed $F(t_-)$ in terms of the error function. To show this, we have to substitute the variable of integration $z = L[1 - \frac{i}{s}(\frac{t_-}{\tau_0})^2]$, where

$$\tau_0 = \frac{1}{c}\sqrt{\frac{8B\lambda_0 L}{\pi}} \tag{80}$$

and s is a new purely imaginary variable. Then the integral (79) takes the form

$$F(t_-) \propto \frac{|t_-|}{\tau_0} \int_{i(t_-/\tau_0)^2}^{i\infty} \frac{ds e^{-s}}{s^{3/2}}. \tag{81}$$

In the complex plane s the integration contour can be turned clockwise for 90° to be made parallel to the real axis. At this new integration contour $s = i(\frac{t_-}{\tau_0})^2 + s'$, where $s' = \mathrm{Re}(s)$ is a new real integration variable changing from 0 to ∞:

$$F(t_-) \propto \frac{|t_-|}{\tau_0} \int_0^{\infty} \frac{ds' e^{-s'}}{\left[i\left(\frac{t_-}{\tau}\right)^2 + s'\right]^{3/2}} = 1 + \sqrt{i\pi}\exp\left[i\left(\frac{t_-}{\tau_0}\right)^2\right]\frac{t_-}{\tau_0}\left[-1 + \mathrm{erf}\left(\sqrt{i}\frac{|t_-|}{\tau_0}\right)\right], \tag{82}$$

where, as usual, all constant and phase factors are dropped. Correctness of the last transformation in Eq. (82) (transition to the error function) can be checked, e.g., by direct calculation of the integral in Mathematica. The normalized squared absolute value of $F(t_-)$ [Eq. (82)] is plotted in Fig. 11 as a function of the dimensionless variable t_-/τ_0.

As the dependence of the function $F(t_-)$ on all parameters of the crystal and pump is concentrated only in the scaling factor τ_0 [Eq. (80)], the curve of Fig. 11 is universal and valid for all values of these parameters under the only condition that pump pulses are long, $\tau \gg LA/c$. In particular, this curve and the analytical results of Eqs. (78) and (82) are perfectly valid for the above considered case of 2-ps long

pulses, for which the temporal wave packets are described in Fig. 9.

Found from Eqs. (78) and (82), single-particle and coincidence widths of the temporal distribution of photons are given by

$$\Delta t_1^{(s)} = \tau \quad \text{and} \quad \Delta t_1^{(c)} = 0.555\tau_0 = \frac{0.555}{c}\sqrt{\frac{8BL\lambda_0}{\pi}}, \tag{83}$$

where 0.555 is the FWHM of the curve in Fig. 11. In contrast to the case of short pulses, in the regime of long pulses of the pump wave the coincidence width $\Delta t_1^{(c)}$ does not depend on t_2. For these reasons, Eqs. (83) can be used for determining the entanglement parameter R_t in the temporal representation:

$$R_t = \frac{\Delta t_1^{(s)}}{\Delta t_1^{(c)}} = \frac{c\tau}{0.555}\sqrt{\frac{\pi}{8BL\lambda_0}} \approx 0.75R_{\text{long}} \approx 0.94K_{\text{long}}, \tag{84}$$

where R_{long} is the R parameter [Eq. (26)] calculated for long pulses in the frequency representation and K_{long} [Eq. (41)] is the above-calculated Schmidt number in the long-pulse asymptotic regime. As seen from Eq. (84), the temporal R parameter, R_t, has all the same functional dependences as R_{long} and K_{long} and slightly differs from them in numerical coefficients. Moreover, R_t appears to be strikingly close to the Schmidt number K_{long}, and this confirms once again a good quality of the R parameter as the entanglement quantifier.

The coincidence width $\Delta t_1^{(c)}$ [Eq. (83)], or equal to it "scaling factor" τ_0 [Eq. (80)], can be interpreted as the correlation time of photons in the biphoton pair. It is important to emphasize that this time does not depend on the pump-pulse duration τ. Hence the correlation time remains finite even in the case of an infinitely long pulse or a purely monochromatic pump. The only reason for a finite time of correlation in the case of long pump pulses is the dispersion. If the dispersion constant B formally tends to zero, the correlation time τ_0 tends to zero too.

Note also that, owing to the assumption that pump pulses are long, in this limit the temporal walk-off appears to be completely switched off. The scaling duration τ_0 [Eq. (80)], as well as the width and all structure of the curve in Fig. 11 are determined only by the dispersion constant B, rather than by any combination of B and A as it was shown to occur in the case of short pulses. Finally, the structure of the curve in Fig. 9 reminds one quite strongly that the structure of the coincidence curves for short pulses in the region of the peak [Fig. 7(b)] and in zone III of Fig. 10. This resemblance is related to the increasing role of dispersion and decreasing role of the temporal walk-off in the cases when a short-pulse pump exits the crystal.

VII. CONCLUSION

Let us summarize here our main results.

(1) For the degenerate collinear type-I SPDC process the parameter R, characterizing the degree of spectral entanglement, is found and shown to be large at any values of pulse duration τ of the pump. Even in the most unfavorable conditions $\tau \sim 1$ ps, where $R(\tau)$ has a minimum, its value does not fall below 70, i.e., $R(\tau) \geqslant R_{\min} \gg 1$.

(2) The control parameter η [Eq. (14)] separating the regions of short and long pulses is found to be determined by the ratio of the double pump-pulse duration to the difference of times during which a crystal is crossed by the pump and idler-signal photons.

(3) By using fundamental features of the biphoton spectral wave function we managed to find the Schmidt number K in the cases of short and long pulses (compared to 1 ps), though the wave function was taken in the form significantly different from the double-Gaussian one. By comparing R and K, we found that they are very close to each other. All functional dependences of R and K are identical, and the difference in numerical coefficients does not exceed 20%. For the class of bipartite wave functions we consider, we found a simple universal formula [Eq. (49)] establishing a relation between R and K for any values of the control parameter η. This means that as soon as the parameter R is measured and η is evaluated, the Schmidt number can be easily found too.

(4) In the temporal picture, a structure of the two-time biphoton wave packet $|\Psi(\tilde{t}_1,\tilde{t}_2)|^2$ is investigated both numerically and analytically (the latter with the help of a series of very simple formulas we have derived), in both cases of short and long pump pulses. It is found that in these two cases (short and long pump pulses) the shapes and localization regions of the temporal biphoton wave packet are significantly different. In the case of long pump pulses the localization region of $|\Psi(\tilde{t}_1,\tilde{t}_2)|^2$ is more or less usual: it looks like a long and thin cigar elongated along the diagonal $\tilde{t}_1 = \tilde{t}_2$ in the plane $(\tilde{t}_1,\tilde{t}_2)$ [Fig. 9(b)]. In contrast to this, in the case of short pump pulses, the localization region of $|\Psi(\tilde{t}_1,\tilde{t}_2)|^2$ is found to be wedge-shaped (Figs. 5 and 10). Again, this "wedge" is elongated along the diagonal $\tilde{t}_1 = \tilde{t}_2$; but, very unusual, its width in the perpendicular direction $(\tilde{t}_1 = -\tilde{t}_2)$ changes in very wide limits. In our example used above, for estimates, from about 1.5 ps in a wide part of the "wedge" down to a few femtoseconds in the narrow part.

(5) The above-described structure of the temporal wave packet in the case of short pump pulses gives rise to the following specific features of the single-particle signals. (a) Duration of the single-particle signal is much longer than that of the pump (~ 3 ps in our example compared to $\tau = 50$ fs). (b) The front wing of the single-particle signal is anomalously long, ~ 1 ps, whereas the rear wing is as short as the pump pulse itself. (c) In its middle part, the envelope of the single-particle signal has the form of a plateau, i.e., is constant. The long duration of the single-particle signal is related to the temporal walk-off effect only, whereas its plateau shape and a long front wing are related to a combined action of the temporal walk-off and dispersion.

(6) In the same case of short pump pulses, coincidence signals have a duration which depends strongly on the observation time. Soon enough after the first signal-idler photons arrival to the end of the crystal, the duration of coincidence signals (equal to the characteristic time of photon correlation in a pair) is very long (~ 1 ps), whereas close to the end of

observability the duration of coincidence signals correlation time becomes very short (a few fs). This uncertainty in the definition of the coincidence duration makes the temporal picture in the case of short pump pulses very inconvenient and inappropriate for defining the R parameter and evaluating in such a way the degree of entanglement of a biphoton state.

(7) In the case of long pulses the wave packet $|\tilde{\Psi}(\tilde{t}_1,\tilde{t}_2)|^2$ is concentrated along the diagonal $\tilde{t}_1=\tilde{t}_2$ and is very narrow and long. The duration of coincidence signals is small, determined purely by dispersion, and independent of the observation time, i.e., constant. Owing to the last reason, the parameter R can be clearly and unambiguously defined, and it appears to be very close to the Schmidt number. Actually, a high degree of closeness between the parameters R and K repeats itself symmetrically in the cases of (a) short pulses and frequency representation and (b) long pulses and temporal representation. In both cases, with a good accuracy, $R=K\gg 1$.

ACKNOWLEDGMENTS

We are grateful to S.P. Kulik and J.H. Eberly for stimulating discussions. The work was supported partially by RFBR Grants No. 05-02-16469 and No. 08-02-01404, the Dynasty Foundation, and the Russian Federation President's Grant No. MK1283.2005.2.

[1] M. V. Fedorov, M. A. Efremov, P. A. Volkov, E. V. Moreva, S. S. Straupe, and S. P. Kulik, Phys. Rev. Lett. **99**, 063901 (2007); Phys. Rev. A **77**, 032336 (2008).
[2] M. B. Nasr *et al.*, Opt. Commun. **246**, 521 (2005).
[3] R. A. O'Donnell and A. B. URen, Opt. Lett. **32**, 817 (2007).
[4] M. V. Fedorov, M. A. Efremov, A. E. Kazakov, K. W. Chan, C. K. Law, and J. H. Eberly, Phys. Rev. A **69**, 052117 (2004).
[5] M. V. Fedorov, M. A. Efremov, P. A. Volkov, and J. H. Eberly, J. Phys. B **39**, S467 (2006).
[6] M. H. Rubin, Phys. Rev. A **54**, 5349 (1996).
[7] A. V. Burlakov, M. V. Chekhova, D. N. Klyshko, S. P. Kulik, A. N. Penin, Y. H. Shih, and D. V. Strekalov, Phys. Rev. A **56**, 3214 (1997).
[8] M. H. Rubin, D. N. Klyshko, Y. H. Shih, and A. V. Sergienko, Phys. Rev. A **50**, 5122 (1994).
[9] T. E. Keller and M. H. Rubin, Phys. Rev. A **56**, 1534 (1997).
[10] H. S. Poh, C. Y. Lum, I. Marcikic, A. Lamas-Linares, and C. Kurtsiefer, Phys. Rev. A **75**, 043816 (2007).
[11] C. K. Law, I. A. Walmsley, and J. H. Eberly, Phys. Rev. Lett. **84**, 5304 (2000).
[12] W. P. Grice and I. A. Walmsley, Phys. Rev. A **56**, 1627 (1997).
[13] G. Di Giuseppe, L. Haiberger, F. De Martini, and A. V. Sergienko, Phys. Rev. A **56**, R21 (1997).
[14] W. P. Grice, R. Erdmann, I. A. Walmsley, and D. Branning, Phys. Rev. A **57**, R2289 (1998).
[15] Y.-H. Kim, V. Berardi, M. V. Chekhova, and Y. Shih, Phys. Rev. A **64**, 011801(R) (2001).
[16] Y.-H. Kim, J. Opt. Soc. Am. B **20**, 1959 (2003).
[17] P. J. Mosley, J. S. Lundeen, B. J. Smith, P. Wasylczyk, A. B. U'Ren, Ch. Silberhorn, and I. A. Walmsley, Phys. Rev. Lett. **100**, 133601 (2008).
[18] W. Mauerer and C. Silberhorn (to be published).
[19] Yu. M. Mikhailova, P. A. Volkov, and M. V. Fedorov, e-print arXiv:0801.0689v1 [quant-ph].
[20] Y. H. Kim, S. P. Kulik, and Y. Shih, Phys. Rev. A **62**, 011802(R) (2000).